

## Self-activating nuclease and anticancer activities of copper(II) complexes with aryl-modified 2,6-di(thiazol-2-yl)pyridine†

Cite this: *Dalton Trans.*, 2013, **42**, 11576

Lüying Li,<sup>a</sup> Kejie Du,<sup>a</sup> Yi Wang,<sup>a</sup> Haina Jia,<sup>a</sup> Xiaojuan Hou,<sup>a,b</sup> Hui Chao<sup>\*a</sup> and Liangnian Ji<sup>\*a</sup>

Three mononuclear copper complexes [Cu(PDTP)Cl<sub>2</sub>] (PDTP = 4-phenyl-2,6-di(thiazole-2-yl)pyridine, **CuPDTP**), [Cu(ADTP)Cl<sub>2</sub>] (ADTP = 4-(anthracen-9-yl)-2,6-di(thiazole-2-yl)pyridine, **CuADTP**) and [Cu(BFDTP)Cl<sub>2</sub>] (BFDTP = 4-(benzofuran-2-yl)-2,6-di(thiazole-2-yl)pyridine, **CuBFDTP**) were synthesized and characterized. The X-ray single crystallography results indicated that the Cu(II) ions showed slightly distorted square pyramidal coordination environments, and the ligands deviated from ideal planarity in all three compounds. Based on the DNA binding studies, it was demonstrated that these three complexes exhibited weak DNA binding strengths, which were most likely groove binding modes. **CuPDTP**, **CuADTP** and **CuBFDTP** induced efficient DNA cleavage in the dark without the addition of external catalysts (oxidant or reductant). In contrast, in the presence of reducing or oxidizing agents, the nuclease activities increased more than 10-fold. Mechanistic investigations revealed the participation of reactive oxygen species, which can be trapped by ROS radical scavengers and ROS sensors. In the same experimental conditions, the free ligands and CuCl<sub>2</sub> did not display any DNA cleaving activity. This result indicates that the complexes, rather than their components, play a significant role in the nuclease reaction process and that DNA cleavage may be initiated in an oxidative pattern. The proposed mechanism was attributed to the *in situ* activation of molecular oxygen by the oxidation of the copper complexes. In the MTT cytotoxicity studies, the three Cu(II) complexes exhibited an antitumor activity against the HeLa, BEL-7402 and HepG2 tumor cell lines. The HeLa cells treated with Cu(II) complexes demonstrated marked changes in their nuclear morphology, which were detected by Hoechst 33258 nuclear staining and acridine orange/ethidium bromide (AO/EB) staining assays. Nuclear chromatin cleavage also was observed from alkaline single-cell gel electrophoresis (comet assay).

Received 9th February 2013,  
Accepted 31st May 2013

DOI: 10.1039/c3dt50395j

[www.rsc.org/dalton](http://www.rsc.org/dalton)

### Introduction

Since the bis-phenanthroline copper complex Cu(phen)<sub>2</sub><sup>2+</sup> was first reported as an effective DNA cleaving agent,<sup>1</sup> copper-based chemical nucleases have attracted significant attention. A number of artificial nucleases containing redox-active Cu(II) as their active sites have been synthesized.<sup>2,3</sup> Copper(II) complexes possess diverse structures and have a reactivity that enables them to effectively cleave DNA and RNA, which gives

them potential value in the treatment of cancer and for applications in biotechnology. Generally, metal-mediated DNA cleavage occurs through one of three different pathways, including photocleavage,<sup>4,5</sup> DNA hydrolysis<sup>6</sup> and oxidative cleavage.<sup>7</sup> Photoactivated DNA cleavage is limited by the effectiveness of the light penetration and the dark toxicity in photodynamic therapy, and metal hydrolases tend to show low cleaving efficiency.<sup>8,9</sup> Thus, synthetic chemical nucleases exhibiting oxidative activity are the main focus of the majority of studies on artificial DNases.<sup>10</sup> The 1,10-phenanthroline copper complex [Cu(phen)<sub>2</sub>]<sup>2+</sup> was reported to oxidatively cleave DNA in the presence of H<sub>2</sub>O<sub>2</sub> by forming “oxo”-Cu(III) active species.<sup>11</sup> Guo *et al.* reported a very active oxidative system of multinuclear copper complexes with the ability to cleave DNA using reductants.<sup>12–14</sup> However, as pharmaceutical agents, these efficient oxidative cleavers require the addition of external reagents (*e.g.*, ascorbic acid or hydrogen peroxide) to initiate the desired reactions, which limits their applications

<sup>a</sup>MOE Key Laboratory of Bioinorganic and Synthetic Chemistry, State Key Laboratory of Optoelectronic Materials and Technologies, School of Chemistry and Chemical Engineering, Sun Yat-Sen University, Guangzhou 510275, P. R. China.

E-mail: ceschh@mail.sysu.edu.cn, cesjln@mail.sysu.edu.cn

<sup>b</sup>Huaihua Medical College, Huaihua 418000, P. R. China

†Electronic supplementary information (ESI) available: Fig. S1–S10. CCDC numbers 869871, 869872 and 869873. For ESI and crystallographic data in CIF or other electronic format see DOI: 10.1039/c3dt50395j

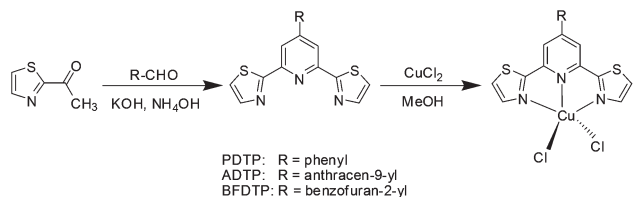
*in vivo*.<sup>9,15</sup> As a result, the development of a self-activating system requiring no further activation to induce the double-strand breakage of DNA is desired.

Recently, copper complexes possessing inherently diverse structural and redox properties have become attractive agents for DNA cleavage due to their potential self-activating nuclease activity.<sup>16–24</sup> Some copper complexes containing hydroxyl-rich ligands or phthalate ligands have the ability to spontaneously generate active oxygen by reactions involving concomitant copper and ligand redox cycles, which initiate DNA cleavage.<sup>16,17</sup> Reedijk *et al.* found that a copper–Hpyramol complex cleaved DNA in the absence of reductants by attacking multiple nucleotide sites.<sup>18,19</sup> In this case, it was suggested that DNA cleavage was initiated by the dehydrogenation of the ligand upon metal center coordination with the participation of non-diffusible radicals. Although the detailed cleavage mechanism remains unclear, all of the reactions appear to be activated by ligand-based metal ions. In the field of clinical anti-tumor treatment, bleomycin (BLM) was observed to trigger both single and double-strand DNA cleavage.<sup>25</sup> In the presence of Fe(II) and O<sub>2</sub>, BLM induces DNA damage without any external reductant by the formation of Fe–OOH, which is an activated intermediate.<sup>26</sup> In the structure, bisthiazole, which is a unit of BLM, is a DNA binding domain that significantly enhances the DNA binding affinity and efficiently promotes the cleavage of two strands of DNA.<sup>27,28</sup> The title Cu(II) complexes, [Cu(PDTP)Cl<sub>2</sub>] (PDTP = 4-phenyl-2,6-di(thiazole-2-yl)pyridine, **CuPDTP**), [Cu(ADTP)Cl<sub>2</sub>] (ADTP = 4-(anthracen-9-yl)-2,6-di(thiazole-2-yl)pyridine, **CuADTP**) and [Cu(BFDTP)Cl<sub>2</sub>] (BFDTP = 4-(benzofuran-2-yl)-2,6-di(thiazole-2-yl)pyridine, **CuBFDTP**), were inspired by BLM and are similar to other thiazole-containing synthetic DNA nucleases.<sup>29,30</sup> Coordinated to the copper, the thiazole ligands were designed and synthesized to be applicable in the study of self-activating nuclease activity. Considering that the majority of the current copper complexes must be initiated by an excess of exogenous agents to cleave DNA, the present work is the first example of thiazole ligand-containing copper complexes that exhibit self-activating oxidative cleavage.

## Results and discussion

### Synthesis and characterization

The methods used to prepare the ligands and complexes are shown in Scheme 1. The ligands were synthesized according to the literature<sup>31</sup> with small modifications. The solution of aryl



**Scheme 1** The synthesis of the ligands and the Cu(II) complexes.

aldehydes and 2-acetylthiazole was stirred for several hours at room temperature. This one-pot method is facile and readily applied to the synthesis of pyridine derivatives containing sterically hindered aryl substitutions. The Cu(II) complexes were prepared in high yields by mixing stoichiometric amounts of CuCl<sub>2</sub>·2H<sub>2</sub>O and the tridentate ligands PDTP, ADTP or BFDTP in a methanol solution. The elemental analyses of all the complexes are in agreement with the corresponding molecular formula. The compositions of the complexes have been further confirmed by their ES-MS spectra. In the mass spectra, the molecular ion [M – Cl]<sup>+</sup> was observed, and the measured molecular weights were consistent with the expected values.

**CuPDTP**, **CuADTP** and **CuBFDTP** were characterized by X-ray single crystallography. The Cu(II) center was found to be coordinated by one N atom (N2) from pyridine and two N atoms (N1, N3) from the dithiazole of the ligands. An ORTEP perspective view is shown in Fig. 1. The coordination geometry of Cu in the complex is described as a distorted square pyramid according to the Addison–Reedijk geometric

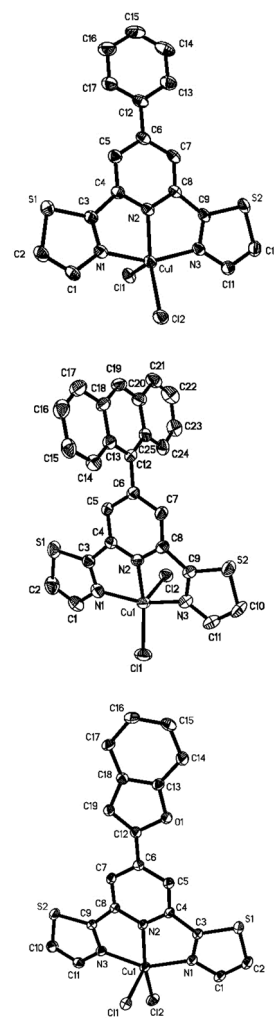


**Fig. 1** ORTEP representations of the complex cations, **CuPDTP** (top), **CuADTP** (middle) and **CuBFDTP** (bottom) showing 30% probability ellipsoid plots.

criterion<sup>32</sup> in which the parameter  $\tau$ , calculated using the observed L–M–L' basal angles, is an index of the degree of trigonality of the structure. Within the structural continuum between the trigonal bipyramidal and square pyramidal limiting geometries,  $\tau$  is equal to zero for a perfect square pyramidal or tetragonal geometry;  $\tau$  becomes unity for a perfect trigonal bipyramidal arrangement. Based on this calculation,  $\tau = 0.015$ , 0.13 and 0.094 for **CuPDTP**, **CuADTP** and **CuBFDTP**, respectively. **CuPDTP** crystallizes in the monoclinic space group ( $P2_1/m$ ). Each asymmetric unit contains two Cu(II) ions, two PDTP ligands and four chloride ions. **CuADTP** and **CuBFDTP** crystallize in the orthorhombic and triclinic space groups, respectively. The coordination geometries of **CuADTP** and **CuBFDTP** are similar to that of **CuPDTP**. The equatorial positions of the distorted square pyramids are occupied by one chloride atom and a ADTP/BFDTP ligand, while the axial position is occupied by another chloride atom. The Cu–N and Cu–Cl bond distances are in the normal range for this coordination geometry. Due to the constrained bite of the tridentate ligands, the Cu–N bond length to the central ring [Cu–N<sub>2</sub> = 1.977(3)–1.995(4) Å] is shorter than those to the terminal rings [2.035(3)–2.068(4) Å], which is typical for the coordination of conjugated terimine systems.<sup>33–35</sup>

The coordination angles reflect the strong distortion caused by the bulk hindrance of the ligand. The dihedral angles of dithiazole and pyridine are 6° and 1°, indicating that the DTP ligand, which contains two thiazoles and a pyridine, shows good planarity. Thus, to discuss the planarity of the ligand, the focus should be directed to their different substitutional groups. In these three compounds, the dihedral angles between pyridine and phenyl, anthracen-9-yl or benzofuran-2-yl are 10°, 78° and 5°, respectively. These results suggest that the overall planarity of the ligands decreases as follows: **CuBFDTP** > **CuPDTP** >> **CuADTP**.

### DNA binding

The three Cu(II) complexes were non-emissive in aqueous solution and in the presence of calf thymus DNA. Hence, the binding of the Cu(II) complexes with DNA cannot be directly presented in the emission spectra. It has been previously reported that the enhanced fluorescence can be quenched, at least partially, by the addition of a second molecule.<sup>36–38</sup> Ethidium bromide (EB) emits intense fluorescence in the presence of DNA, and the extent of the fluorescence quenching of EB bound to DNA is used to determine the extent of the binding between the second molecule and the DNA.<sup>37</sup> The fluorescence quenching of EB bound to DNA by the Cu(II) complexes is shown in Fig. 2. The ability of the present complexes to quench the EB emission decreased in the order of **CuBFDTP** (37.1%) > **CuPDTP** (29.8%) > **CuADTP** (10.8%). Compared with DNA intercalative Cu(II) complexes,<sup>38</sup> these slight changes in fluorescence indicated that the Cu(II) complexes cannot displace the EB molecules from the DNA base pairs, suggesting the primarily electrostatic or groove DNA binding<sup>39</sup> nature of the Cu(II) complexes.

According to previous reports,<sup>40,41</sup> the intercalation of the metallointercalators generally results in prominent increases

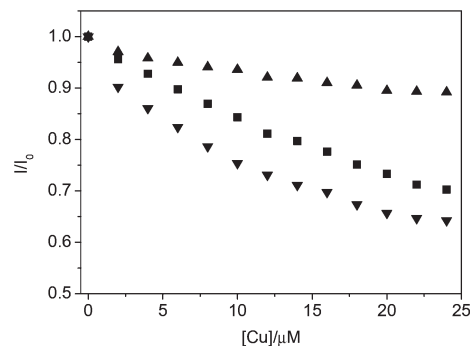


**Fig. 2** The emission profiles of 100  $\mu\text{M}$  CT-DNA-bound EB in a 10 mM phosphate buffer (pH 7.2) at room temperature upon the addition of **CuPDTP** (■), **CuADTP** (▲), **CuBFDTP** (▼). [EB] = 10  $\mu\text{M}$ , [Cu] = 0–24  $\mu\text{M}$ .

in the DNA melting temperature ( $T_m$ ). The melting curves of CT-DNA in the absence and presence of **CuPDTP**, **CuADTP** and **CuBFDTP** are presented in Fig. S1 (ESI†). The thermal denaturation profiles of native DNA in the presence of the Cu(II) complexes, obtained by plotting the UV absorbance at 258 nm as a function of temperature, show that the DNA melting temperature decreased by 1.1, 2.3, and 0.8 °C, respectively. This indicates that **CuPDTP**, **CuADTP** and **CuBFDTP** may bind to the DNA in groove sites and destabilize the DNA helix. This is observation is different from that seen when DNA-intercalative metal complexes bind to DNA, as DNA-intercalative metal complexes stabilize the double helix.<sup>36,40,41</sup> The small decreases in the DNA denaturation temperature ( $\Delta T_m$ ) in the presence of **CuPDTP**, **CuADTP** and **CuBFDTP** further verify the conclusion obtained in the EB displacement assay.

Circular dichroic spectral studies provide information regarding the DNA conformational changes as well as the interaction strength between the metal complexes and DNA. The CD spectrum of CT-DNA exhibits a positive band at 275 nm due to base stacking and a negative band at 245 nm due to the right-handed helicity of the B-DNA form, which is quite sensitive to the mode of DNA interaction with small molecules. The simple groove binding and electrostatic interaction of the complexes with DNA show less or no perturbation of the base stacking and helicity bands, while the intercalator enhances the intensities of both bands.<sup>42–44</sup> From the CD spectra (Fig. S2, ESI†), it was observed that the DNA CD bands were weakly modified by increasing amounts of the Cu(II) complexes, confirming that the double helical structure is only slightly perturbed by the interaction with the Cu(II) complexes. This observation was consistent with the above spectroscopic studies. Given that the nuclease activity was not affected by high salt concentrations (Fig. S3, ESI†), we speculate that the Cu(II) complexes do not bind the DNA through electrostatic interactions. Similar to the oxidative cleaving agent  $[\text{Cu}(\text{phen})_2]^{2+}$ ,<sup>45</sup> the Cu(II) complexes likely interact with the DNA through groove binding.

### Chemical nuclease activity

The cleavage of plasmid pBR322 DNA induced by **CuPDTP**, **CuADTP** and **CuBFDTP** was performed in the absence of

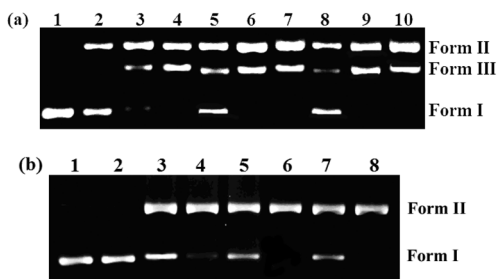


**Fig. 3** The gel electrophoresis of pBR322 DNA cleavage catalyzed by **CuPDTP**, **CuADTP** and **CuBFDTP** in phosphate buffer at 37 °C for 1.5 h. (a) Lane 1: DNA control (40  $\mu$ M), lanes 2–4: DNA + **CuPDTP** (25, 50, 100  $\mu$ M), lanes 5–7: DNA + **CuADTP** (25, 50, 100  $\mu$ M), lanes 8–10: DNA + **CuBFDTP** (25, 50, 100  $\mu$ M). (b) Lane 1: DNA control (40  $\mu$ M); lane 2: DNA +  $\text{H}_2\text{O}_2$  (100  $\mu$ M); lanes 3 and 4: DNA + **CuPDTP** (5, 10  $\mu$ M) +  $\text{H}_2\text{O}_2$  (100  $\mu$ M); lanes 5 and 6: DNA + **CuADTP** (5, 10  $\mu$ M) +  $\text{H}_2\text{O}_2$  (100  $\mu$ M); lanes 7 and 8: DNA + **CuBFDTP** (5, 10  $\mu$ M) +  $\text{H}_2\text{O}_2$  (100  $\mu$ M).

external cofactor agents (either oxidant or reductant) in the dark. The Cu(II) complexes were found to promote the cleavage of plasmid pBR322 DNA from the supercoiled form (I) to the nicked form (II) and linear form (III) (Fig. 3a). No DNA cleavage was observed for the control in which the metal complex was absent (lane 1). When the concentrations of the three Cu(II) complexes were increased (lanes 2–10), the amount of form I of pBR322 DNA diminished gradually, whereas the amounts of form II and III increased. The Cu(II) complexes are able to induce significant cleavage of the plasmid DNA at the concentration of 25  $\mu$ M. At the concentration of 100  $\mu$ M, **CuPDTP**, **CuADTP** and **CuBFDTP** almost promote the complete conversion of DNA from form I to forms II and III. Similar cases were also observed in the light or in an argon atmosphere (Fig. S4, ESI<sup>†</sup>). In the presence of an oxidant (100  $\mu$ M  $\text{H}_2\text{O}_2$ ) under aerobic conditions (Fig. 3b), only 5  $\mu$ M of **CuPDTP**, **CuADTP** and **CuBFDTP** can degrade 60–80% of DNA. In the presence of a reducing agent (250  $\mu$ M ascorbic acid), 10  $\mu$ M of the Cu(II) complexes are sufficient to induce 60–70% of the plasmid DNA cleavage (Fig. 4). This observation indicates that the chemical nuclease activities of the Cu(II) complexes are significantly promoted with the addition of either oxidants or reductants.

The DNA groove binding preference of the complexes was studied using the DNA major groove binder methyl green and the DNA minor groove binder distamycin. A significant inhibition in the chemical nuclease activity of complexes **CuPDTP**, **CuADTP** and **CuBFDTP** was observed in the presence of

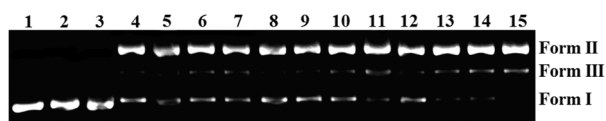


**Fig. 4** The agarose gel electrophoresis of the Cu(II) complexes showing the oxidative cleavage of DNA in the presence of ascorbic acid (HA, 250  $\mu$ M). Lane 1: DNA control (40  $\mu$ M); lane 2: DNA + HA; lane 3: DNA +  $\text{CuCl}_2$  (500  $\mu$ M) + HA; lanes 4–7: DNA + **CuPDTP** (5, 10, 15, 20  $\mu$ M) + HA; lanes 8–11: DNA + **CuADTP** (5, 10, 15, 20  $\mu$ M) + HA; lanes 12–15: DNA + **CuBFDTP** (5, 10, 15, 20  $\mu$ M) + HA.

distamycin (100  $\mu$ M), while the methyl green (100  $\mu$ M) addition has no apparent effect on the DNA cleavage of these complexes. The results indicate the minor groove binding propensity of **CuPDTP**, **CuADTP** and **CuBFDTP** (Fig. S5, ESI<sup>†</sup>). The DNA cleavage experiments were performed at different pH values (pH = 5.5–9.5) and it was found that the pH of the solution exhibited little effect on the DNA cleavage activity of the Cu(II) complexes (Fig. S6, ESI<sup>†</sup>). It was also noticed that in the presence of the thiazole ligands, **CuPDTP**, **CuADTP** and **CuBFDTP** can exhibit self-activating oxidative cleavage; however, when replacing the thiazole with pyridine, such a behavior was not observed in the Cu(II) complexes (Fig. S7, ESI<sup>†</sup>).

Similar to DNA enzymes,<sup>46</sup> DNA cleavage induced by **CuPDTP**, **CuADTP** and **CuBFDTP** is dependent on temperature and time. At 37 °C, all of the Cu(II) complexes demonstrated significantly higher nuclease activities than at lower temperatures (Fig. S8, ESI<sup>†</sup>). This result follows the trend that cleavage reactions are more active at higher temperatures. The cleavage efficiency was also enhanced with time (Fig. 5); the amounts of plasmid DNA gradually decreased due to the degradation of the SC DNA (form I) to the NC form (form II) and L DNA (form III). The double-strand DNA cleavage was completed within 2 h and the plasmid DNA ultimately disappeared. The kinetic characterization of the DNA cleavage by **CuPDTP**, **CuADTP** and **CuBFDTP** showed that the time-dependent disappearance of form I DNA and the appearance of form II and form III DNA followed pseudo-first-order kinetic profiles (Fig. 5b).<sup>47</sup> However, these profiles cannot be fitted with a single exponential function (Fig. S9, ESI<sup>†</sup>). This result indicates that the cleavage did not occur through a simple hydrolytic pathway. Furthermore, the DNA cleavage products failed to be religated by the enzyme T4 DNA ligase, giving additional evidence of nonhydrolysis. Additionally, all of the experiments were performed in dark, so the action of photo-induced cleavage can be excluded. All of the observations support the

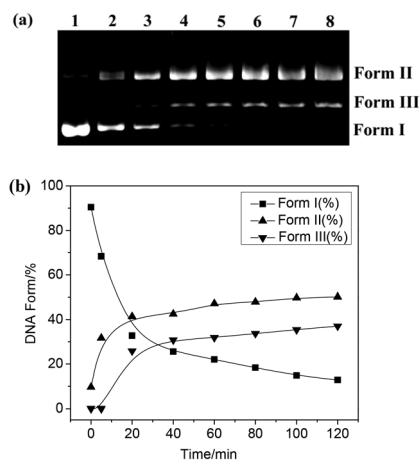


**Fig. 5** (a) Time-dependent experiments of pBR322 DNA (40  $\mu$ M bp) cleavage catalyzed by **CuBFDTP** (20  $\mu$ M) over a period of 120 min at 37 °C in phosphate buffer (pH 7.0). Lane 1: DNA control (40  $\mu$ M), lanes 2–8: DNA + 20  $\mu$ M **CuBFDTP** (incubating time 5, 20, 40, 60, 80, 100, 120 min). (b) A plot of the changes of form I, form II and form III with time.

hypothesis that **CuPDTP**, **CuADTP** and **CuBFDTP** most likely cleaved the plasmid DNA by a self-activating oxidative mechanism, which is similar to the manner in which bleomycin cooperates with a redox metal ( $\text{Fe}^{\text{II}}$ ) to trigger DNA cleavage without exogenous agents.

### A mechanistic investigation of the DNA cleavage reaction

To explore the cleavage mechanism, the copper-mediated DNA cleavage was investigated with several different potential radical scavengers to identify the intermediate reactive oxygen species (ROS) in the absence of external cofactors (Fig. 6 and Fig. S10, ESI†). DMSO and mannitol were used as hydroxyl radical ( $\text{HO}^\cdot$ ) scavengers; sodium azide and L-histidine were used as singlet oxygen ( $^1\text{O}_2$ ) scavengers; and superoxide dismutase (SOD) was used as an  $\text{O}_2^{\cdot-}$  radical scavenger. The DNA breaks mediated by **CuPDTP**, **CuADTP** and **CuBFDTP** were not affected by the presence of the hydroxyl radical inhibitors DMSO and mannitol, suggesting that diffusible hydroxyl radicals were not involved in the DNA damage mechanism. The single oxygen scavengers  $\text{NaN}_3$  and histidine partially decreased the cleavage activity, each to a different extent. Sodium azide was significantly more effective than histidine, which is likely due to the  $\text{NaN}_3$  chelation of the metal ion, which indicates that singlet oxygen may participate in the nuclease reaction. However, in the dark, it was observed that the singlet oxygen scavengers  $\text{NaN}_3$  and histidine had no effect on the cleavage activity (Fig. S11, ESI†). The metal chelator EDTA also completely inhibited cleavage activity, indicating that this DNA cleavage mechanism is a metal-assisted reaction. DNA cleaving activity is completely repressed by catalase, an enzyme that disproportionates  $\text{H}_2\text{O}_2$  to yield  $\text{H}_2\text{O} + \text{O}_2$ ,<sup>48</sup> implying that  $\text{H}_2\text{O}_2$  as a reactive oxygen species is responsible for DNA cleavage. In contrast, SOD, an enzyme capable of converting the superoxide radical to  $\text{H}_2\text{O}_2$ , promotes DNA damage. This is additional proof that  $\text{H}_2\text{O}_2$  participates in the cleavage. The cleavage is not dependent on the carbon scavenger 2,2,6,6-tetramethyl-1-piperidinyloxy (TEMPO), ruling out the existence of a carbon radical in the reaction. The ROS inhibitor studies have indicated that DNA cleavage can be initiated by reactive oxygen species  $^1\text{O}_2$  (only in the light) and  $\text{H}_2\text{O}_2$  but not diffusing  $\text{OH}^\cdot$  radicals. Considering that these types of active species mostly occur in oxidative cleavage, it is

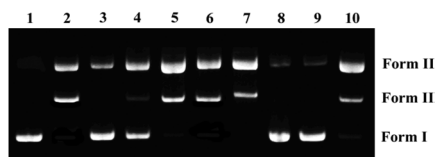


**Fig. 6** The agarose gel electrophoresis of **CuBFDTP** (100  $\mu\text{M}$ ) cleaving DNA (40  $\mu\text{M}$ ) in the presence of various radical scavengers under "self-activating" conditions for 1.5 h at 37  $^\circ\text{C}$ . (a) Lane 1: DNA control; lane 2: no inhibitor ( $[\text{CuBFDTP}] = 100 \mu\text{M}$ ); lane 3: **CuBFDTP** +  $\text{NaN}_3$  (100 mM); lane 4: **CuBFDTP** + histidine (100 mM); lane 5: **CuBFDTP** + DMSO (100 mM); lane 6: **CuBFDTP** + mannitol (50 mM); lane 7: **CuBFDTP** + SOD (500  $\text{U mL}^{-1}$ ); lane 8: **CuBFDTP** + catalase (1000  $\text{U mL}^{-1}$ ); lane 9: **CuBFDTP** + EDTA (10 mM); lane 10: **CuBFDTP** + TEMPO (20 mM).

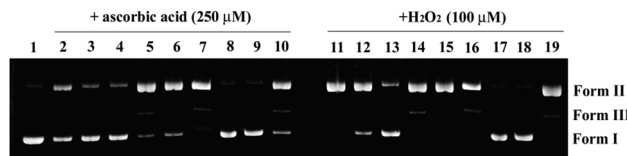


**Fig. 7** The agarose gel electrophoresis of **CuBFDTP** (10  $\mu\text{M}$ ) cleaving DNA (40  $\mu\text{M}$ ) in the presence of various radical scavengers under redox conditions for 1.5 h at 37  $^\circ\text{C}$ . Lane 1: DNA control, lanes 2 and 11: no inhibitor ( $[\text{CuBFDTP}] = 10 \mu\text{M}$ ); lanes 3 and 12: **CuBFDTP** +  $\text{NaN}_3$  (100 mM); lanes 4 and 13: **CuBFDTP** + histidine (100 mM); lanes 5 and 14: **CuBFDTP** + DMSO (100 mM); lanes 6 and 15: **CuBFDTP** + mannitol (50 mM); lanes 7 and 16: **CuBFDTP** + SOD (500  $\text{U mL}^{-1}$ ); lanes 8 and 17: **CuBFDTP** + catalase (1000  $\text{U mL}^{-1}$ ); lanes 9 and 18: **CuBFDTP** + EDTA (10 mM); lanes 10 and 19: **CuBFDTP** + TEMPO (20 mM).

most likely that **CuPDTP**, **CuADTP** and **CuBFDTP** cleaved the DNA through a self-activating oxidative pathway.

To further test the involvement of  $\text{H}_2\text{O}_2$  in the cleavage reaction, parallel cleavage experiments were performed. Under redox reaction conditions, **CuPDTP**, **CuADTP** and **CuBFDTP** were found to form the same ROS species involved in the reaction, and  $\text{H}_2\text{O}_2$  was the crucial active intermediate involved in the DNA cleavage (Fig. 7 and Fig. S12, ESI†). The resulting nuclease activity and mechanism under redox conditions strongly indicate a "self-activating" mechanism, which is most likely initiated by the copper(II) complex through an oxidative pathway.<sup>49–51</sup> However, under the present conditions, because the high valent copper species were unstable, evidence for  $\text{CuBFDTP}^+$  was difficult to observe. Further studies are currently underway to clarify the cleavage mechanism.

### The detection of reactive oxygen species

The ROS radical also was detected by various radical indicators. The possibility of hydroxyl radical formation in the presence of the copper complexes was evaluated using rhodamine B dye. This reaction was performed in a 10 mM phosphate buffer at pH 7.2 under aerobic conditions. Based on our observation, there was no obvious decrease in the absorbance of the dye at 552 nm in the presence of the copper complexes (Fig. S13a, ESI†). The electronic spectra of rhodamine B was slightly increased after incubation with **CuADTP** due to the assembly of a copper complex in the rhodamine B solution. Under the same conditions, a parallel experiment, using  $\text{FeCl}_2$  and  $\text{H}_2\text{O}_2$  (the Fenton conditions),<sup>16</sup> displayed a gradual decrease with the reaction time, verifying that the hydroxyl radical formation resulted in dye degradation. The diffusing hydroxyl radicals were not trapped during the detection of rhodamine B degradation, suggesting that the  $\text{OH}^\cdot$  radical was not included in the reaction. Unlike the  $\text{H}_2\text{O}_2$  and  $\text{O}_2$  activating copper nuclease, which produces  $\text{OH}^\cdot$  by an internal electron transfer to initiate DNA cleavage,<sup>52</sup> **CuPDTP**, **CuADTP** and **CuBFDTP** cleaved DNA without the participation of  $\text{OH}^\cdot$  radicals.

When using 1,3-diphenylisobenzofuran (DPBF),<sup>53</sup> the emission is quenched in the presence of  $^1\text{O}_2$ . The changes in the dye emission can be used to evaluate the formation of  $^1\text{O}_2$ . In a typical experiment, DPBF was incubated with the  $\text{Cu}(\text{II})$  complexes while monitoring the fluorescence at 479 nm. The DPBF

fluorescence consumption *vs.* time profile is shown in Fig. S13b (ESI<sup>†</sup>). As a positive control, the emission of DPBF with [Ru(bpy)<sub>3</sub>]<sup>2+</sup> under aerobic conditions resulted in a decrease in the fluorescence intensity of DPBF. This indicates that the dye was consumed in the presence of the singlet oxygen radicals under aerobic conditions. Similar to [Ru(bpy)<sub>3</sub>]<sup>2+</sup>, **CuPDTP**, **CuADTP** and **CuBFDTP** resulted in decreased fluorescence of DPBF with time, indicating the formation of <sup>1</sup>O<sub>2</sub> in the reaction system.

To test whether the H<sub>2</sub>O<sub>2</sub> intermediate was formed by the copper complexes in aqueous solution, 2',7'-dichlorofluorescein (DCF) was examined for the formation of H<sub>2</sub>O<sub>2</sub>.<sup>54</sup> The nonfluorescent DCFH can be rapidly oxidized to emit the strongly fluorescent DCF in the presence of H<sub>2</sub>O<sub>2</sub>. In our experiment, when incubated with **CuPDTP**, **CuADTP** and **CuBFDTP**, DCFH consistently generated significant fluorescence (Fig. S13c, ESI<sup>†</sup>). **CuADTP** showed the highest H<sub>2</sub>O<sub>2</sub> quantum yield and exhibiting the strongest amount of emission. In the negative contrasting experiment, the DCFH dye was pre-incubated with catalase (1000 U mL<sup>-1</sup>) to remove H<sub>2</sub>O<sub>2</sub>. To our surprise, the fluorescence intensity did not change significantly. The observations indicated that the oxidation of DCFH was directly inhibited by the addition of catalase. This result provided additional proof that H<sub>2</sub>O<sub>2</sub> is an active intermediate that is generated in the reaction system and that it is an active species with respect to catalyzed DNA cleavage.

### Cytotoxicity

The cytotoxicities of **CuPDTP**, **CuADTP** and **CuBFDTP** were measured using a standard MTT assay<sup>55</sup> against three human-derived tumor cell lines with the clinical anti-tumor agent cisplatin as a control. Under similar conditions, the target complexes were tested on HeLa human cervix carcinoma cell lines, BEL-7402 and the HepG2 hepatoma carcinoma cell line. The IC<sub>50</sub> values for the cell lines incubated with the complexes are summarized in Table 1. **CuPDTP**, **CuADTP** and **CuBFDTP** displayed medium toxicities against all three tumor lines, and in all cases, the activities of the complexes were higher than those of the corresponding free ligands. The cytotoxic activity studies *in vitro* indicate that the Cu(II) complexes have excellent activities on the BEL-7402 and HepG2 cells but showed a significantly lower activity than cisplatin for the HeLa cells (IC<sub>50</sub> = 0.014 mM, which was calculated by the same experimental method). Hence, the above results indicate that the Cu(II) complexes are active on specific cancer cells. The better cytotoxic

**Table 1** The IC<sub>50</sub> values (mM) for the Cu(II) complexes and cisplatin against cervical cancer cells (HeLa), hepatoma carcinoma cells (BEL-7402) and hepatocellular carcinoma cells (HepG2) over a period of 24 h

	IC <sub>50</sub> (mM)			
	Cisplatin	<b>CuPDTP</b>	<b>CuADTP</b>	<b>CuBFDTP</b>
HeLa	0.014	0.059	0.036	0.043
BEL-7402	0.020	0.028	0.021	0.026
HepG2	0.026	0.036	0.027	0.033

activity of the Cu(II) complex may be attributed to its stronger ability to cleave DNA. The findings of the *in vitro* cytotoxic activities further confirm that the DNA cleavage induced by Cu(II) complexes leads to cell death.

### Nuclear morphology

Cell death can be divided into two types, necrosis (accidental cell death) and apoptosis (programmed cell death).<sup>56</sup> Necrotic cells undergo cell lysis and lose their membrane integrity, inducing severe inflammation.<sup>57</sup> Apoptotic cells, however, are transformed into small membrane-bound vesicles (apoptotic bodies), which are engulfed *in vivo* by macrophages, and no inflammatory response is found.<sup>58</sup> The harmless removal of cells (*e.g.*, cancer cells) is one consideration in chemotherapy.<sup>59</sup> Therefore, the induction of apoptosis is one of the considerations in the development of anticancer drugs. To identify the possible involvement of apoptosis, HeLa cells treated with the Cu(II) complexes were stained with Hoechst 33258.<sup>60</sup> As shown in Fig. 8 for the HeLa cells treated with **CuPDTP**, **CuADTP** and **CuBFDTP**, a significant increase in the apoptotic nuclear morphology, such as extensive chromatin aggregation or nuclear condensation, was observed in the treated cells; in contrast, the nuclear contours of normal HeLa cells stained with Hoechst 33258 stained evenly. The number of abnormal cells generated at 24 h varied according to **CuADTP** > **CuBFDTP** > **CuPDTP**. The higher apoptosis-inducing activity of **CuADTP** is consistent with its stronger double-strand DNA cleavage ability.

It is well-established that acridine orange (AO) is able to penetrate the membranes of viable cells, while EB is excluded. Therefore, the emission of green fluorescence from AO is a convenient marker for viable cells, and the emission of red fluorescence from EB indicates a loss of cell viability.<sup>61</sup> Microphotographs of the AO/EB-stained HeLa cells, which were pretreated for 24 h with the three Cu(II) complexes, showed that **CuPDTP**, **CuADTP** and **CuBFDTP** induced the apoptosis of the HeLa cells (Fig. 9). Some of the apoptotic cells were also detected in secondary necrosis. As shown, the three Cu(II)

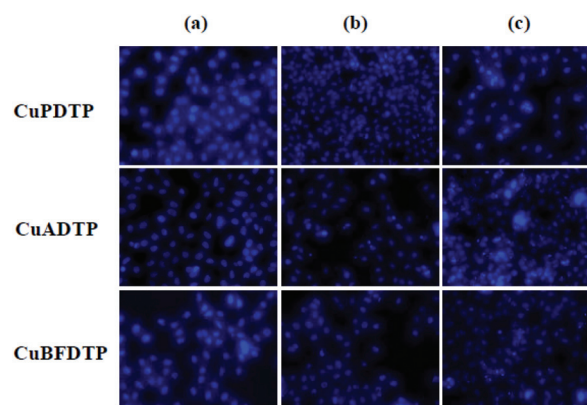


**Fig. 8** HeLa cells were stained with Hoechst 33258 and observed under a fluorescence microscope: (a) untreated cells, (b) treated with the Cu(II) complexes (25 μM), (c) treated with the Cu(II) complexes (50 μM).

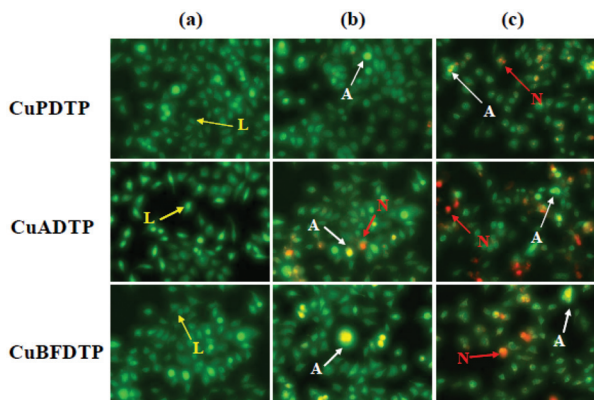


**Fig. 9** HeLa cells were stained by AO/EB and observed under a fluorescence microscope: (a) untreated cells, (b) treated with the Cu(II) complexes (25  $\mu\text{M}$ ), (c) treated with the Cu(II) complexes (50  $\mu\text{M}$ ); incubated at 37  $^{\circ}\text{C}$  and 5%  $\text{CO}_2$  for 24 h. The arrows point to the cells representing certain cell viability status: L points to the live cells; A points to the apoptotic cells; and N points to the necrotic cells.

complexes (15  $\mu\text{M}$ ) can induce apoptosis, which is observed as the condensation of the HeLa cell nuclei after 24 h. Upon the treatment of the cells with significant amounts of the Cu(II) complexes (60  $\mu\text{M}$ ), the cells exhibited condensed orange nuclei (Fig. 9), which is a hallmark of late apoptotic cells; however, the necrotic cells displayed structurally intact nuclei with even orange staining. The orange nucleus was due to the loss of membrane integrity in the late apoptotic and necrotic cells, allowing EB to stain the nucleus. The results further support the idea that the CuPDTP, CuADTP and CuBFDTP complexes caused significant HeLa cell apoptosis. The morphological changes observed with CuPDTP, CuADTP and CuBFDTP suggest that the cells are committed to death in such a way that both apoptotic and necrotic cells increase in number in a concentration-dependent manner. The ability of the Cu(II) complexes to induce apoptotic cell death is consistent with the results from the Hoechst 33258 staining.

### Comet assay

Our present experiment has clearly shown that these Cu(II) complexes induced DNA strand cleavage by generating ROS such as  $^1\text{O}_2$  and  $\text{H}_2\text{O}_2$ . Additionally, this mechanism is believed to be the molecular basis of their cytotoxic activity. Alkaline single-cell gel electrophoresis (comet assay) can give a perspective of the changes that occur in the chromatin organization within a single cell, which is considered a more accurate way of detecting early nuclear changes in a cell population.<sup>62</sup> For example, as shown in Fig. 10, no broom-like tails were observed in the untreated cells (Fig. 10a). Treatment with 15  $\mu\text{M}$  Cu(II) complex led to the appearance of obscure “halos” around the nuclei of the HeLa cells (Fig. 10b), illustrating that DNA damage occurred in these cells; additionally, when 30  $\mu\text{M}$  Cu(II) complex was introduced, the nuclei began to shrink (Fig. 10c). At Cu(II) complex concentrations of up to 60  $\mu\text{M}$ , a sudden change could be observed: the nuclei almost disappeared, and this was further accompanied by the

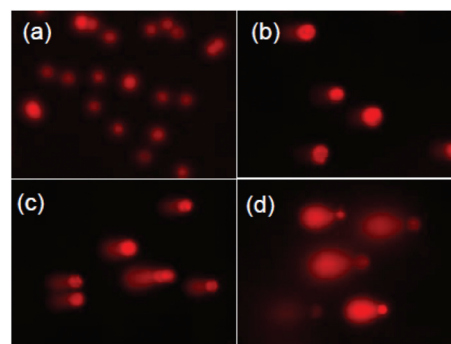


**Fig. 10** Drug-induced double-strand DNA breaks in HeLa cells. Cells were untreated (a) or treated with (b) CuADTP (15  $\mu\text{M}$ ), (c) CuADTP (30  $\mu\text{M}$ ), (d) CuADTP (60  $\mu\text{M}$ ) for 2 h. The detection of the DNA breaks was done using alkaline single-cell gel electrophoresis.

appearance of “broom-like” tails, indicating the presence of severe DNA damage (Fig. 10d). The outcome of the comet assay showed that the DNA of a single cell underwent degradation as a consequence of direct DNA damage or rapid apoptosis. The high level of DNA damage induced by the Cu(II) complexes reinforces the above results obtained using the MTT assay and the nuclear staining assay.

### The intracellular reactive oxygen species study

To elucidate the relationship between cytotoxicity and the generation of reactive oxygen species (ROS), CuPDTP, CuADTP and CuBFDTP were exposed to HeLa human cervix carcinoma cancer cells, which had been pre-treated with the intracellular ROS indicator 2',7'-dichlorofluorescein diacetate (DCFH-DA). In the presence of endogenously generated ROS, DCFH-DA is oxidized to release the fluorophore 2',7'-dichlorofluorescein (DCF).<sup>54</sup> The results show an increase in the cellular ROS levels after treatment for 12 h with the complexes and are expressed in comparison to the ROS levels of the unexposed controls (Fig. 11). The amount of the intracellular ROS species

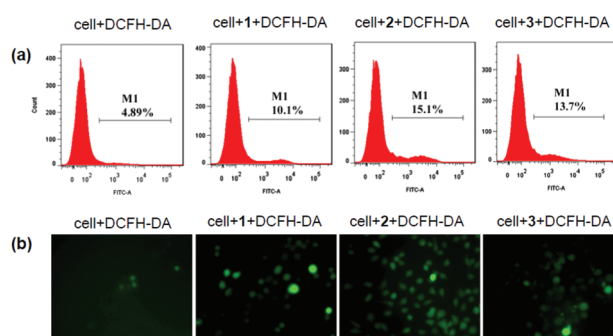


**Fig. 11** The DCFH-DA detection of the ROS in HeLa cells treated with the Cu(II) complexes CuPDTP (1), CuADTP (2) and CuBFDTP (3). The HeLa cells were incubated with the Cu(II) complexes for 12 h, which was followed by incubation with 10  $\mu\text{M}$  DCFH-DA for 30 min. (a) The level of intracellular ROS was detected by a DCFH-DA assay using flow cytometric analysis. The percentage of ROS-over-expressing cells under different treatments was detected. (b) HeLa cells showing an increase in the ROS level when treated with the Cu(II) complexes viewed using a fluorescence microscope.

generated by the Cu(II) complexes follows the order of **CuADTP** > **CuBFDTP** > **CuPDTP**, which is the same as that observed for the IC<sub>50</sub> values. This reveals that **CuADTP**, which exhibits the strongest double-strand DNA cleavage ability, activates the ROS-generating machinery and generates the highest amount of ROS when treated with cancer cells, leading to apoptosis. Thus, it is clear that the Cu(II) complexes act as efficient anti-cancer agents by an oxidative stress mechanism.

## Conclusions

In conclusion, the Cu(II) complexes **CuPDTP**, **CuADTP** and **CuBFDTP**, possessing an extensive heterogeneous ring, present an impressive plasmid DNA cleaving ability, which triggers double-strand DNA breaks in the absence of any exogenous oxidants or reductants. After groove binding with DNA, the complexes cleaved the DNA strands by a self-activating oxidative mechanism involving the generation of ROS. It is proposed that molecular oxygen is reduced to hydrogen peroxide *in situ* in a mechanism that is likely initiated by the redox of Cu(II) during self-activating oxidative cleavage. The three Cu(II) complexes show high antitumor activities to HeLa, BEL-7402 and HepG2 tumor cells. Nuclear chromatin cleavage has been observed from Hoechst 33258 and AO/EB staining assays. Alkaline single-cell gel electrophoresis (comet assay) provides evidence that the Cu(II) complexes indeed induce DNA fragmentation, which is further evidence of apoptosis. We hope the results will be of value in further understanding the DNA cleavage and damage induced by Cu(II) complexes, as well as laying the foundations for the discovery of new antitumor drugs.

## Experimental section

### Materials

2-Acetylthiazole, benzaldehyde, anthracen-9-yl-carboxaldehyde, and CuCl<sub>2</sub>·2H<sub>2</sub>O were purchased from Alfa Aesar. Calf thymus DNA and supercoiled plasmid pBR322 DNA were purchased from Sigma and Fermentas, respectively. Ultrapure water was used for all experiments. 2',7'-Dichlorofluorescein (DCFH) and 1,3-diphenylisobenzofuran (DPBF) were purchased from Sigma. The agarose gels and ethidium bromide (EB) were purchased from Sangon. T4 DNA ligase, agarose, a gel DNA Extraction Kit and EcoRI endonuclease were purchased from Takara Co., Ltd. All commercial solvents were used without further purification.

### Physical measurements

Elemental analyses (C, H and N) were carried out using a Vario EL elemental analyzer. <sup>1</sup>H NMR spectra were recorded using a Varian Mercury-Plus 300 NMR spectrometer or a Varian INOVA500NB 500 NMR spectrometer with (CD<sub>3</sub>)<sub>2</sub>SO as the solvent at room temperature and TMS as the internal standard. Electrospray mass spectra (ES-MS) were recorded using an LCQ

system (Finnigan MAT, USA), and the quoted *m/z* values given in this work are for the major peaks in the isotope distribution. UV-visible (UV-vis) spectra were recorded using a Perkin-Elmer Lambda 850 spectrophotometer, and the fluorescence spectra were recorded using a Perkin-Elmer LS55 Fluorescence spectrometer. CD spectra were measured using a JASCO-J810 spectrometer equipped with a Peltier temperature-controlling programmer (±0.1 °C).

### The synthesis of 4-phenyl-2,6-di(thiazole-2-yl)pyridine (PDTP)

2-Acetylthiazole (1.28 g, 10 mmol) was added into a solution of benzaldehyde (0.53 g, 5 mmol) in EtOH (10 mL). KOH pellets (0.77 g, 85%, 10 mmol) and NH<sub>3</sub> (aq., 1.49 mL, 25%, 20 mmol) were then added to the mixture. After stirring at room temperature for 4 h, a silver-white solid was collected by filtration and washed with EtOH (3 × 10 mL). The yield was 81%. The ligand was used in the next step to obtain the copper complex without further purification. Anal. calcd for C<sub>17</sub>H<sub>11</sub>N<sub>3</sub>S<sub>2</sub> (%): C, 63.53; H, 3.45; N, 13.07; found (%): C, 63.51; H, 3.46; N, 13.02. ES-MS (CH<sub>3</sub>OH) *m/z*: 322 [M + H]<sup>+</sup>. <sup>1</sup>H NMR (500 MHz, d<sub>6</sub>-DMSO): δ 8.42 (s, 1H); 8.08 (d, 2H, *J* = 6 Hz); 7.96 (d, 2H, *J* = 6 Hz); 7.94 (d, 2H, *J* = 7 Hz); 7.58 (dd, 1H, *J* = 8 Hz); 7.56 (dd, 2H, *J* = 7 Hz).

### The synthesis of 4-(anthracen-9-yl)-2,6-di(thiazole-2-yl)pyridine (ADTP)

Anthracen-9-yl-carboxaldehyde (1.03 g, 5 mmol) was dissolved in an EtOH (20 mL) solution for 1 h, and then 2-acetylthiazole (1.28 g, 10 mmol), KOH (0.77 g, 85%, 10 mmol) and NH<sub>3</sub> (aq., 1.49 mL, 25%, 20 mmol) were added to the system. After stirring at room temperature overnight, a brown powder was collected by filtration and washed with excess ethanol (3 × 10 mL). The yield was 65%. Anal. calcd for C<sub>25</sub>H<sub>15</sub>N<sub>3</sub>S<sub>2</sub> (%): C, 71.23; H, 3.59; N, 9.97; found (%): C, 71.18; H, 3.62; N, 9.96. ES-MS (CH<sub>3</sub>OH) *m/z*: 422 [M + H]<sup>+</sup>. <sup>1</sup>H NMR (500 MHz, d<sub>6</sub>-DMSO): δ 8.32 (dd, 2H, *J* = 8 Hz); 8.22 (m, 2H); 8.18 (s, 2H); 8.01 (dd, 2H, *J* = 7.5 Hz); 8.69 (d, 1H, *J* = 8.8 Hz); 7.61 (m, 4H); 7.50 (m, 2H).

### The synthesis of 4-(benzofuran-2-yl)-2,6-di(thiazole-2-yl)pyridine (BFDTP)

This compound (pale yellow) was synthesized in an identical manner to that described for PDTP using benzo[*b*]furan-2-carboxaldehyde (0.73 g, 5 mmol) in place of benzaldehyde. The yield was 55%. Anal. calcd for C<sub>19</sub>H<sub>11</sub>N<sub>3</sub>OS<sub>2</sub> (%): C, 63.14; H, 3.07; N, 11.63; found (%): C, 63.11; H, 3.12; N, 11.60. ES-MS (CH<sub>3</sub>OH) *m/z*: 362 [M + H]<sup>+</sup>. <sup>1</sup>H NMR (500 MHz, d<sub>6</sub>-DMSO): δ 8.58 (s, 2H); 8.09 (d, 2H, *J* = 6 Hz); 8.03 (s, 1H); 7.97 (d, 2H, *J* = 6 Hz); 7.76 (d, 2H, *J* = 8 Hz); 7.46 (d, 1H, *J* = 7 Hz); 7.35 (t, 1H, *J* = 5 Hz).

### The synthesis of Cu(PDTP)Cl<sub>2</sub> (CuPDTP)

The ligand PDTP (0.322 g, 1 mmol) was dissolved in 20 mL methanol solution, and CuCl<sub>2</sub>·2H<sub>2</sub>O (0.17 g, 1 mmol) in methanol was added dropwise to the solution. After stirring the mixture for 4 h at 50 °C, the solution turned clear green.

The resulting solution was filtered while it was hot, and the filtrate was left unperturbed in air to allow slow evaporation. Dark-green crystals were obtained after one week. The yield was 62%. Anal. calcd for  $C_{17}H_{11}Cl_2N_3S_2Cu$  (%): C, 44.79; H, 2.43; N, 9.22; found (%): C, 44.75; H, 2.46; N, 9.19. ES-MS ( $CH_3OH$ )  $m/z$ : 421  $[M - Cl]^+$ . UV-vis spectra (DMSO) [ $\lambda_{max}$ , nm ( $\epsilon$ ,  $M^{-1} cm^{-1}$ )]: 292 (34 900), 334 (21 500).

### The synthesis of $Cu(ADTP)Cl_2$ (CuADTP)

The ADTP ligand is poorly soluble in methanol; thus, the use of a prolonged stirring time was required to dissolve the ligand. ADTP (0.422 g, 1 mmol) was dissolved in 20 mL methanol. After the ADTP was dissolved completely,  $CuCl_2 \cdot 2H_2O$  (0.17 g, 1 mmol) in methanol was added dropwise to the solution. Stirring was continued for 5 h, and the solution was filtered while it was hot. The filtrate was kept for developing crystals. The yield was 53%. Anal. calcd for  $C_{25}H_{15}Cl_2N_3S_2Cu$  (%): C, 54.01; H, 2.72; N, 7.56; found (%): C, 53.97; H, 2.75; N, 7.54. ES-MS ( $CH_3OH$ )  $m/z$ : 521  $[M - Cl]^+$ . UV-vis spectra (DMSO) [ $\lambda_{max}$ , nm ( $\epsilon$ ,  $M^{-1} cm^{-1}$ )]: 301 (27 900), 331 (20 700), 369 (12 700), 389 (11 700).

### The synthesis of $Cu(BFDTP)Cl_2$ (CuBFDTP)

This compound was synthesized in a manner identical to that described for CuPDTP using BFDTP (0.362 g, 1 mmol) in place of PDTP. Green crystals were collected after 1 week. The yield was 40%. Anal. calcd for  $C_{19}H_{11}Cl_2N_3OS_2Cu$  (%): C, 46.02; H, 2.24; N, 8.47; found (%): C, 45.99; H, 2.28; N, 8.46. ES-MS ( $CH_3OH$ )  $m/z$ : 461  $[M - Cl]^+$ . UV-vis (DMSO) [ $\lambda_{max}$ , nm ( $\epsilon$ ,  $M^{-1} cm^{-1}$ )]: 314 (25 400), 331 (22 100).

### X-ray crystallography

The intensity data were collected using a Bruker Apex CCD area-detector diffractometer (Mo  $K\alpha$ ). Absorption corrections were applied by using a multi-scan program SADABS. The structures were solved with direct methods and were refined

with the full-matrix least-squares technique using the SHELXS 97<sup>63</sup> and SHELXL 97<sup>63</sup> program packages. Anisotropic thermal parameters were applied to all non-hydrogen atoms except the guest molecules. The organic hydrogen atoms were generated geometrically. The crystal data and refinement parameters for the complexes are summarized in Table 2. Selected bond lengths and angles are given in Table 3.

Detailed crystallographic data for the crystal structural analysis have been collected in the Cambridge Crystallographic Data Centre, given by the CCDC reference numbers 869871, 869872 and 869873, which contain the supplementary crystallographic data for the present paper.

### DNA binding experiments

The DNA binding experiments were performed at room temperature. All spectroscopic titration measurements were carried out in a 10 mM phosphate buffer at pH 7.2.

The fluorescence quenching experiments were conducted by adding small aliquots of a 100  $\mu M$  Cu(II) complex solution to samples containing 4  $\mu M$  ethidium bromide (EB) and 80  $\mu M$  DNA in buffer. The samples were excited at 340 nm, and the emission was observed between 500 and 700 nm.

The  $T_m$  was determined by monitoring the UV absorbance of DNA at 260 nm in the absence or presence of the Cu(II) complexes using a Perkin Elmer Lambda-850 UV-vis spectrometer equipped with an auto-temperature controller system. The  $T_m$  was obtained by fitting  $(A - A_0)/(A_f - A_0)$  versus temperature, where  $A_f$ ,  $A_0$  and  $A$  are the final, initial and observed absorbances at 260 nm, respectively.

Circular dichroism spectroscopic studies were performed using a JASCO J-810 automatic recording spectropolarimeter. All determinations were performed at room temperature with 1 cm pathway cells. The CD spectra were run from 400–220 nm at a speed of 100  $nm min^{-1}$ , and the data were recorded at an interval of 0.1 nm. The buffer background was automatically subtracted, and the data were accumulated 3 times and then averaged.

**Table 2** Crystallographic data for CuPDTP, CuADTP and CuBFDTP

	CuPDTP	CuADTP	CuBFDTP
Empirical formula	$C_{17}H_{11}Cl_2CuN_3S_2$	$C_{25}H_{15}Cl_2CuN_3S_2$	$C_{19}H_{11}Cl_2CuN_3OS_2$
Crystal system	Monoclinic	Orthorhombic	Triclinic
Space group	$P2_1/n$	$P2_12_12_1$	$P\bar{1}$
$a/\text{\AA}$	18.5932(18)	10.241(3)	7.9078(11)
$b/\text{\AA}$	8.4641(8)	10.290(3)	11.1470(16)
$c/\text{\AA}$	23.526(2)	23.602(6)	11.5729(16)
$\alpha/^\circ$	90	90	111.368(2)
$\beta/^\circ$	102.327(2)	90	92.003(2)
$\gamma/^\circ$	90	90	90.218(2)
$V/\text{\AA}^3$	3617.1(6)	2487.3(11)	949.3(2)
$Z$	8	4	2
$\mu/\text{mm}^{-1}$	1.739	1.285	1.668
$D_c/\text{g cm}^{-3}$	1.674	1.527	1.735
$\theta$ range ( $^\circ$ )	1.27–26.00	1.73–25.99	1.89–25.99
Unique reflns/ $R_{int}$	7026/0.0338	4883/0.0372	3688/0.0213
Final $R [I > 2\sigma(I)] R_1$	0.0447	0.0496	0.0362
Final $R [I > 2\sigma(I)] wR_2$	0.1094	0.1383	0.0895
$R$ indices (all data) $R_1$	0.0686	0.0609	0.0453
$R$ indices (all data) $wR_2$	0.1318	0.1477	0.0972

**Table 3** Selected bond lengths (Å) and angles (°) for CuPDTP, CuADTP and CuBFDTP

CuPDTP		CuADTP		CuBFDTP	
Cu(1)–N(2)	1.977(3)	Cu(1)–N(2)	1.995(4)	Cu(1)–N(2)	1.987(2)
Cu(1)–N(3)	2.035(3)	Cu(1)–N(3)	2.052(4)	Cu(1)–N(1)	2.054(2)
Cu(1)–N(1)	2.056(3)	Cu(1)–N(1)	2.068(4)	Cu(1)–N(3)	2.053(2)
Cu(1)–Cl(2)	2.2520(11)	Cu(1)–Cl(1)	2.2203(15)	Cu(1)–Cl(2)	2.2307(9)
Cu(1)–Cl(1)	2.4665(11)	Cu(1)–Cl(2)	2.4988(14)	Cu(1)–Cl(1)	2.4556(9)
N(2)–Cu(1)–N(3)	78.26(12)	N(2)–Cu(1)–N(3)	78.14(15)	N(2)–Cu(1)–N(1)	78.01(9)
N(2)–Cu(1)–N(1)	78.05(12)	N(2)–Cu(1)–N(1)	78.71(16)	N(2)–Cu(1)–N(3)	78.18(9)
N(3)–Cu(1)–N(1)	154.30(12)	N(3)–Cu(1)–N(1)	155.36(17)	N(1)–Cu(1)–N(3)	152.75(9)
N(2)–Cu(1)–Cl(2)	155.17(9)	N(2)–Cu(1)–Cl(1)	163.18(12)	N(2)–Cu(1)–Cl(2)	158.36(8)
N(3)–Cu(1)–Cl(2)	99.16(9)	N(3)–Cu(1)–Cl(1)	100.53(12)	N(1)–Cu(1)–Cl(2)	97.76(7)
N(1)–Cu(1)–Cl(2)	98.15(9)	N(1)–Cu(1)–Cl(1)	99.17(13)	N(3)–Cu(1)–Cl(2)	99.48(7)
N(2)–Cu(1)–Cl(1)	100.50(9)	N(2)–Cu(1)–Cl(2)	92.11(12)	N(2)–Cu(1)–Cl(1)	98.57(7)
N(3)–Cu(1)–Cl(1)	98.14(9)	N(3)–Cu(1)–Cl(2)	96.38(12)	N(1)–Cu(1)–Cl(1)	100.39(7)
N(1)–Cu(1)–Cl(1)	95.81(9)	N(1)–Cu(1)–Cl(2)	92.78(13)	N(3)–Cu(1)–Cl(1)	96.09(7)
Cl(2)–Cu(1)–Cl(1)	104.30(4)	Cl(1)–Cu(1)–Cl(2)	104.69(6)	Cl(2)–Cu(1)–Cl(1)	103.06(3)

### Nuclease activities

The reactions were carried out with 40  $\mu\text{M}$  pBR322 DNA and Cu(II) complexes in a 10 mM phosphate buffer at pH 7.2. The copper complexes were initially prepared in DMF, then diluted in phosphate buffer. A fixed amount of DNA was mixed with the copper complex solution and diluted by phosphate buffer to a total volume of 10  $\mu\text{L}$ . In the nuclease activity mechanism studies, different ROS radical scavengers were added to the DNA solution before the complexes. The following procedure is similar to the typical nuclease activity study. The samples were incubated for 1.5 h at 37  $^{\circ}\text{C}$  in the dark, followed by quenching with 2  $\mu\text{L}$  of loading buffer (0.25% bromophenol blue, 1.86% EDTA and 50% glycerol). Electrophoresis was completed at 80 V loading on agarose gel (0.8%) for 1.5 h in TBE buffer (89 mM Tris, 89 mM  $\text{H}_3\text{BO}_3$ , 2 mM EDTA). After staining with an EB solution (1  $\mu\text{g mL}^{-1}$ ), the bands were visualized under UV light and photographed with an Alpha Innotech IS-5500 Chemiimager.

### ROS radical detection experiments

The generation of ROS in the cleavage reaction was detected by dye degradation or by using sensitive radical sensors. Hydroxyl radical formation was quantified by rhodamine B (10  $\mu\text{M}$ ) degraded in the presence of Cu(II) complexes (100  $\mu\text{M}$ ) in phosphate buffer under aerobic conditions. The degradation of the dye was monitored by the UV absorbance of rhodamine B at 552 nm. A parallel experiment was carried out with a mixture of  $\text{FeCl}_2$  (100  $\mu\text{M}$ ) and  $\text{H}_2\text{O}_2$  (10  $\mu\text{M}$ ) (the Fenton conditions) as the control. The control was used to verify that the dye degrades in the presence of hydroxyl radicals.

The fluorescent probes DPBF<sup>53</sup> and DCFH<sup>54</sup> have been reported to detect  $^1\text{O}_2$  and  $\text{H}_2\text{O}_2$ , respectively. These two probes were used to evaluate the ROS species in our experiment.

In the presence of  $^1\text{O}_2$ , DPBF is activated, forming its non-emissive derivative. From the fluorescence measurements, the level of fluorescence consumption can be identified. Mixtures of  $[\text{Ru}(\text{bpy})_3]^{2+}$  or the Cu(II) complexes with DPBF in a

methanol solution were used to monitor the changes in the luminescence as a function of time.  $e_x = 405 \text{ nm}$ ,  $e_m = 479 \text{ nm}$ . As a control experiment,  $[\text{Ru}(\text{bpy})_3]^{2+}$  was reported to generate  $^1\text{O}_2$  as a result of DPBF consumption, which showed a significant decrease in fluorescence. In our experiment, the fluorescence intensity of all the copper complexes was observed to decrease in the presence of DPBF, suggesting the probable formation of  $^1\text{O}_2$  during the nuclease reaction.

Similar to the mechanism of DPBF when used as a  $^1\text{O}_2$  sensor, DCFH is oxidized by  $\text{H}_2\text{O}_2$  and generates dehydro-form 2',7'-dichlorofluorescein (DCF), emitting significant green fluorescence. The  $\text{H}_2\text{O}_2$  radical detection was performed by adding the copper complexes to the DCFH methanol solution and recording the signal changes in fluorescence ( $e_x = 470 \text{ nm}$ ,  $e_m = 525 \text{ nm}$ ). To further verify the involvement of  $\text{H}_2\text{O}_2$  in the cleaving process, the Cu(II) complexes were added to a catalase pre-incubated DCFH solution, and the emission levels were observed. As a negative control system, the catalase–DCFH mixture exhibited insufficient changes in the fluorescence upon the addition of the copper complexes due to the reduction of  $\text{H}_2\text{O}_2$  radicals.

### Cell lines and cell culture

Human cancer cell lines, including cervical carcinoma HeLa and hepatocellular carcinoma HepG2, were purchased from American Type Culture Collection (ATCC, Manassas, VA). The human hepatocellular carcinoma BEL-7402 cell line was obtained from the Cell Bank (Cell Institute, Sinica Academica Shanghai, Shanghai, China). All cell lines were maintained in either RPMI-1640 or DMEM medium supplemented with fetal bovine serum (10%), penicillin (100 units per mL) and streptomycin (50 units per mL) at 37  $^{\circ}\text{C}$  in a  $\text{CO}_2$  incubator (95% relative humidity, 5%  $\text{CO}_2$ ).

### Cytotoxicity

*In vitro* cytotoxicity tests were carried out using a standard MTT (3-(4,5-dimethylthiazole-2-yl)-2,5-diphenyltetrazolium bromide) colorimetric assay.<sup>55</sup> The cells were plated in 96-well microassay culture plates ( $1 \times 10^4$  cells per well) and grown

overnight at 37 °C in a 5% CO<sub>2</sub> incubator. The test compounds were then added to the wells to achieve final concentrations ranging from 10<sup>-6</sup> to 10<sup>-4</sup> M. The control wells were prepared by the addition of culture medium (100 µL). The wells containing culture medium without cells were used as blanks. The plates were incubated at 37 °C in a 5% CO<sub>2</sub> incubator for 48 h. Upon completion of the incubation step, the stock MTT dye solution (20 µL, 5 mg mL<sup>-1</sup>) was added to each well. After 4 h of incubation, buffer (100 µL) containing *N,N*-dimethylformamide (50%) and sodium dodecyl sulfate (20%) was added to solubilize the MTT formazan. The optical density of each well was then measured on a microplate spectrophotometer at a wavelength of 490 nm. The IC<sub>50</sub> value was determined from plots of % viability against the dose of compound added.

#### Hoechst 33258 nuclear staining<sup>60</sup>

The control and the HeLa cells were treated with the Cu(II) complexes at the noted concentrations for 24 h in the dark. At the end of the incubation, the cells attached to the glass plates were washed twice with ice-cold PBS and then were fixed with 4% paraformaldehyde in PBS for 10 min. A solution of Hoechst 33258 (20 µg mL<sup>-1</sup>) was added to stain the cells for 10 min in the dark. After washing twice with PBS, the cells were examined for condensed nuclei under an inverted fluorescence microscope (Zeiss Axio Observer D1).

#### Ethidium bromide/acridine orange (AO/EB) staining<sup>61</sup>

A monolayer of HeLa cells was incubated in the absence or presence of the Cu(II) complexes at a concentration of 50 µM at 37 °C and 5% CO<sub>2</sub> for 24 h. After 24 h, the cells were stained with an AO/EB solution (100 µg mL<sup>-1</sup> AO, 100 µg mL<sup>-1</sup> EB). The samples were observed under an inverted fluorescence microscope (Zeiss Axio Observer D1).

#### Alkaline single-cell gel electrophoresis (comet assay)<sup>62</sup>

An alkaline single-cell gel electrophoresis (comet assay) was performed to measure the extent of DNA fragmentation induced by the Cu(II) complexes in the HeLa cells after 24 h. Briefly, 1 × 10<sup>4</sup> cells per mL of treated and untreated HeLa cells were mixed with 0.8% low-melting-point agarose at a ratio of 1:10 (v/v) and spread on slides precoated with 1% normal agarose. The embedded cells were lysed in a precooled lytic solution (2.5 M NaCl, 100 mM EDTA, 10 mM Tris base and 1% Triton X-100, 10% DMSO; the last two compounds were added fresh, pH 10) at 4 °C for 120 min, rinsed, and equilibrated in an alkaline electrophoresis buffer (0.3 M NaOH and 1 mM EDTA, pH 13). The electrophoresis was performed in an ice bath at 25 V and 300 mA for 20 min, and the slides were neutralized with 0.4 M Tris-HCl (pH 7.5), stained with PI solution (2 µg mL<sup>-1</sup>) for 5 min in the dark and analyzed using an inverted fluorescence microscope (Zeiss Axio Observer D1). The DNA contents in the head and tail were quantified using the "comet score" from Autocomet.

#### Intracellular reactive oxygen species (ROS) measurement

The formation of intracellular ROS in the cells was measured according to the manufacturer's protocol for the Reactive Oxygen Species Assay Kit (Beyotime Institute of Biotechnology, China). The cultured HeLa cells were treated with an IC<sub>50</sub> concentration of the Cu(II) complexes and the untreated cells were maintained as the control. After incubation for 12 h, the cells were harvested and washed twice, then resuspended in 10 µM 2,7-dichlorodihydrofluorescein diacetate (DCFH-DA) and incubated at 37 °C for 30 min. The levels of intracellular ROS were examined with flow cytometry (FACSCanto II, BD Biosciences, USA) and an inverted fluorescence microscope (Zeiss Axio Observer D1). The wavelength of excitation was 485 nm, and the fluorescence was measured at 530 nm. The level of intracellular ROS was expressed as the mean fluorescence intensity. Data acquisition and analysis were performed using BD FACS-Diva software v6.0.

#### Acknowledgements

The authors thank the National Science of Foundation of China (no. 21071155, 21172273, 21171177), the National Science of Foundation of Guangdong Province (9351027501000003), the Research Fund for the Doctoral Program of Higher Education (20110171110013), the State Key Laboratory of Optoelectronic Materials and Technologies (2010-ZY-4-5) and Sun Yat-Sen University for financial support. X. J. H. thanks the support of the Science and Technology Department of Hunan Province (2010FJ4090).

#### Notes and references

- 1 D. S. Sigman, D. R. Graham, V. D. Aurora and A. M. Stern, *J. Biol. Chem.*, 1979, **254**, 12269–12272.
- 2 C. Marzano, M. Pellei, F. Tisato and C. Santini, *Anti-Cancer Agents Med. Chem.*, 2009, **9**, 185–211.
- 3 J. A. Cowan, *Curr. Opin. Chem. Biol.*, 2001, **5**, 634–642.
- 4 T. Bortolotto, P. P. Silva, A. Neves, E. C. Pereira-Maia and H. Terenzi, *Inorg. Chem.*, 2011, **50**, 10519–10521.
- 5 T. K. Goswami, B. V. S. K. Chakravarthi, M. Roy, A. A. Karande and A. R. Chakravarty, *Inorg. Chem.*, 2011, **50**, 8452–8464.
- 6 N. Mitić, S. J. Smith, A. Neves, L. W. Guddat, L. R. Gahan and G. Schenk, *Chem. Rev.*, 2006, **106**, 3338–3363.
- 7 Q. Jiang, N. Xiao, P. F. Shi, Y. G. Zhu and Z. J. Guo, *Coord. Chem. Rev.*, 2007, **251**, 1951.
- 8 L. Tjioe, A. Meininger, T. Joshi, L. Spiccia and B. Graham, *Inorg. Chem.*, 2011, **50**, 4327–1972.
- 9 D. D. Li, F. P. Huang, G. J. Chen, C. Y. Gao, J. L. Tian, W. Gu, X. Liu and S. P. Yan, *J. Inorg. Biochem.*, 2010, **104**, 431–441.
- 10 S. M. Hadi, M. F. Ullah, U. Shamim, S. H. Bhatt and A. S. Azmi, *Chemotherapy*, 2010, **56**, 280–284.

- 11 W. K. Pogozelski and T. D. Tullius, *Chem. Rev.*, 1998, **98**, 1089–1108.
- 12 Y. M. Zhao, J. H. Zhu, W. J. He, Z. Yang, Y. G. Zhu, Y. Z. Li, J. F. Zhang and Z. J. Guo, *Chem.–Eur. J.*, 2006, **12**, 6621–6629.
- 13 J. W. Chen, X. Y. Wang, Y. Shao, J. H. Zhu, Y. G. Zhu, Y. Z. Li, Q. Xu and Z. J. Guo, *Inorg. Chem.*, 2007, **46**, 3306–3312.
- 14 C. Tu, Y. Shao, N. Gan, D. Xu and Z. J. Guo, *Inorg. Chem.*, 2004, **43**, 4761–4766.
- 15 B. K. Santra, P. A. N. Reddy, G. Neelakanta, S. Mahadevan, M. Nethaji and A. R. Chakravarty, *J. Inorg. Biochem.*, 2002, **89**, 191–196.
- 16 S. S. Tonde, A. S. Kumbhar, S. B. Padhye and R. J. Butcher, *J. Inorg. Biochem.*, 2006, **100**, 51–60.
- 17 A. Kellett, M. O'Connor, M. McCann, M. McNamara, P. Lynch, G. Rosair, V. McKee, B. Creaven, M. Walsh, S. McClean, A. Foltyn, D. O'Shea, O. Howe and M. Devereux, *Dalton Trans.*, 2011, **40**, 1024–1027.
- 18 P. U. Maheswari, S. Roy, H. den Dulk, S. Barends, G. P. van Wezel, B. Kozlevčar, P. Gamez and J. Reedijk, *J. Am. Chem. Soc.*, 2006, **128**, 710–711.
- 19 P. U. Maheswari, M. van der Ster, S. Smulders, S. Barends, G. P. van Wezel, C. Massera, S. Roy, H. den Dulk, P. Gamez and J. Reedijk, *Inorg. Chem.*, 2008, **47**, 3719–3727.
- 20 K. Li, L. H. Zhou, J. Zhang, S. Y. Chen, Z. W. Zhang, J. J. Zhang, H. H. Lin and X. Q. Yu, *Eur. J. Med. Chem.*, 2009, **44**, 1768–1772.
- 21 E. Lamour, S. Routier, J. L. Bernier, J. P. Catteau, C. Bailly and H. Vezin, *J. Am. Chem. Soc.*, 1999, **121**, 1862–1869.
- 22 K. Ghosh, P. Kumar, N. Tyagi, U. P. Singh, V. Aggarwal and M. C. Baratto, *Eur. J. Med. Chem.*, 2010, **45**, 3770–3779.
- 23 K. Ghosh, P. Kumar, N. Tyagi, U. P. Singh and N. Goel, *Inorg. Chem. Commun.*, 2011, **14**, 489–492.
- 24 K. Ghosh, P. Kumar, V. Mohan, U. P. Singh, S. Kasiri and S. S. Mandal, *Inorg. Chem.*, 2012, **51**, 3343–3345.
- 25 R. M. Burger, *Chem. Rev.*, 1998, **98**, 1153–1170.
- 26 L. Worth, B. L. Frank, D. F. Christner, M. J. Absalon, J. Stubbe and J. W. Kozarich, *Biochemistry*, 1993, **32**, 2601–2609.
- 27 S. J. Sucheck, J. F. Ellena and S. M. Hecht, *J. Am. Chem. Soc.*, 1998, **120**, 7450–7460.
- 28 A. T. Abraham, X. Zhou and S. M. Hecht, *J. Am. Chem. Soc.*, 2001, **123**, 5167–5175.
- 29 H. Sasaki, *Chem. Pharm. Bull.*, 2007, **55**, 1762–1767.
- 30 M. Gras, B. Therrien, G. Suss-Fink, A. Casini, F. Edefe and P. J. Dyson, *J. Organomet. Chem.*, 2010, **695**, 1119–1125.
- 31 J. H. Wang and G. S. Hanan, *Synlett*, 2005, 1251–1254.
- 32 A. W. Addison, T. N. Rao, J. Reedijk, J. van Rijn and C. C. Verschoor, *J. Chem. Soc., Dalton Trans.*, 1984, 1349–1356.
- 33 G. D. Storrer, S. B. Colbran and D. C. Craig, *J. Chem. Soc., Dalton Trans.*, 1998, 1351–1364.
- 34 N. W. Alock, P. R. Barker, J. M. Haider, M. J. Hannon, C. L. Painting, Z. Pikramenou, E. A. Plummer, K. Rissanen and P. Saarenketo, *J. Chem. Soc., Dalton Trans.*, 2000, 1447–1462.
- 35 H. Chao, G. Yang, G. Q. Xue, H. Li, H. Zhang, I. D. Williams, L. N. Ji, X. M. Chen and X. Y. Li, *J. Chem. Soc., Dalton Trans.*, 2001, 1326–1331.
- 36 M. J. Waring, *J. Mol. Biol.*, 1965, **13**, 269–282.
- 37 C. L. Liu, J. Y. Zhou and H. B. Xu, *J. Inorg. Biochem.*, 1998, **71**, 1–6.
- 38 X. L. Wang, H. Chao, H. Li, X. L. Hong, L. N. Ji and X. Y. Li, *J. Inorg. Biochem.*, 2004, **98**, 423–429.
- 39 G. Yang, J. Z. Wu, L. Wang, L. N. Ji and X. Tian, *J. Inorg. Biochem.*, 1997, **66**, 141–144.
- 40 G. A. Neyhart, N. Grover, S. R. Smith, W. A. Kalsbeck, T. A. Fairly, M. Cory and H. H. Thorp, *J. Am. Chem. Soc.*, 1993, **115**, 4423–4428.
- 41 F. Gao, H. Chao, F. Zhou, X. Chen, Y. F. Wei and L. N. Ji, *J. Inorg. Biochem.*, 2008, **102**, 1050–1059.
- 42 S. Mahadevan and M. Palaniandavar, *Inorg. Chem.*, 1998, **37**, 3927–3934.
- 43 B. Saha, M. M. Islam, S. Paul, S. Samanta, S. Ray, C. R. Santra, S. R. Choudhury, B. Dey, A. Das, S. Ghosh, S. Mukhopadhyay, G. S. Kumar and P. Karmakar, *J. Phys. Chem. B*, 2010, **114**, 5851–5861.
- 44 L. Y. Li, H. N. Jia, H. J. Yu, K. J. Du, Q. T. Lin, K. Q. Qiu, H. Chao and L. N. Ji, *J. Inorg. Biochem.*, 2012, **113**, 31–39.
- 45 T. B. Thederahn, M. D. Kuwabara, T. A. Larsen and D. S. Sigman, *J. Am. Chem. Soc.*, 1989, **111**, 4941–4946.
- 46 A. Sreedhara, J. D. Freed and J. A. Cowan, *J. Am. Chem. Soc.*, 2000, **122**, 8814–8824.
- 47 J. T. Wang, Q. Xia, X. H. Zheng, H. Y. Chen, H. Chao, Z. W. Mao and L. N. Ji, *Dalton Trans.*, 2010, **39**, 2128–2136.
- 48 S. Borah, M. S. Melvin, N. Lindquist and R. A. Manderville, *J. Am. Chem. Soc.*, 1998, **120**, 4557–4562.
- 49 J. A. Cowan, *Curr. Opin. Chem. Biol.*, 2001, **5**, 634–642.
- 50 Y. Jin and J. A. Cowan, *J. Am. Chem. Soc.*, 2005, **127**, 8408–8415.
- 51 S. Mahapatra, J. A. Halfen, E. C. Wilkinson, L. Que Jr. and W. B. Tolman, *J. Am. Chem. Soc.*, 1994, **116**, 9785–9786.
- 52 Q. Zhu, Y. Lian, S. Thyagarajan, S. E. Rokita, K. D. Karlin and N. V. Blough, *J. Am. Chem. Soc.*, 2008, **130**, 6304–6305.
- 53 H. J. Yu, S. M. Huang, L. Y. Li, H. N. Jia, H. Chao, Z. W. Mao, J. Z. Liu and L. N. Ji, *J. Inorg. Biochem.*, 2009, **103**, 881–890.
- 54 L. R. Silveira, L. Pereira-Da-Silva, C. Juel and Y. Hellsten, *Free Radical Biol. Med.*, 2003, **35**, 455–464.
- 55 T. Mosmann, *J. Immunol. Methods*, 1983, **65**, 55–63.
- 56 I. Vermees and C. Haanen, *Adv. Clin. Chem.*, 1984, **31**, 177–246.
- 57 R. van Furth and T. L. Van Zwet, *J. Immunol. Methods*, 1988, **108**, 45–51.
- 58 J. S. Savill, P. M. Henson, J. E. Henson, C. Haslett, M. J. Walport and A. H. Wyllie, *J. Clin. Invest.*, 1989, **83**, 865–875.

- 59 N. A. Thornberry and Y. Lazebnik, *Science*, 1998, **281**, 1312–1316.
- 60 S. Chen, J. Lin, S. Liu, Y. Liang and S. Lin-Shiau, *Toxicol. Sci.*, 2008, **102**, 138–149.
- 61 G. P. Amarante-Mendes, E. Bossy-Wetzel, T. Brunner, D. Finucane, D. R. Green and S. Kasibhatla, in *Cells: A laboratory manual*, ed. D. L. Spector, R. D. Goldman and L. A. Leinwand, Cold Spring Harbor Laboratory Press, New York, ch. 15, vol. 1, 1998.
- 62 A. Stang and I. Witte, *Mutat. Res., Genet. Toxicol. Environ. Mutagen.*, 2009, **675**, 5–10.
- 63 G. M. Sheldrick, *Acta Crystallogr., Sect. A: Found. Crystallogr.*, 2008, **64**, 112–122.